Published in final edited form as:

Langmuir. 2019 November 26; 35(47): 15232–15241. doi:10.1021/acs.langmuir.9b02590.

Cholesterol regulates the incorporation and catalytic activity of tissue-nonspecific alkaline phosphatase in DPPC monolayers

R. Derradi[1], **M. Bolean**[1], **A.M.S. Simão**[1], **L. Caseli**[2], **J.L. Millán**[3], **M. Bottini**[*,3,4], **P. Ciancaglini**[1], **A.P. Ramos**[*,1]

[1]Chemistry Department, Faculty of Philosophy, Sciences and Letters at Ribeirao Preto, Department of Chemistry, University of Sao Paulo, Avenida Bandeirantes, 3900, Monte Alegre, Ribeirao Preto, SP, Brazil, 14040-901

[2]Institute of Environmental, Chemical and Pharmaceutical Sciences, Federal University of Sao Paulo, Rua Sao Nicolau, 210, Centro, Diadema, SP, Brazil, 09913-030

[3]Sanford Burnham Prebys Medical Discovery Institute, La Jolla, CA 92037, USA

[4]Department of Experimental Medicine, University of Rome Tor Vergata, 00133 Rome, Italy.

Abstract

Matrix vesicles (MVs) are a special class of extracellular vesicles that drive bone and dentin mineralization by providing the essential enzymes and ions for the nucleation and propagation of mineral crystals. Tissue-nonspecific alkaline phosphatase (TNAP) is an integral protein of MV membrane and participates in biomineralization by hydrolyzing extracellular pyrophosphate (PP_i) – a strong mineralization inhibitor – and forming inorganic phosphate (P_i) necessary for the growth of mineral crystals inside MVs and their propagation once released in the extracellular matrix. MV membrane is enriched in cholesterol (CHOL), which influences the incorporation and activity of integral proteins in biologic membranes, however how CHOL controls the incorporation and activity of TNAP in MV membrane has not yet been elucidated. In the present study, Langmuir monolayers were used as a MV membrane biomimetic model to assess how CHOL affects TNAP incorporation and activity. Surface pressure-area (π-A) isotherms of binary dipalmitoilphosphatidylcholine (DPPC)/CHOL monolayers showed that TNAP incorporation increases with CHOL concentration. Infrared spectroscopy showed that CHOL influences the conformation and orientation of the enzyme. Optical-fluorescence micrographs of the monolayers revealed the tendency of TNAP to incorporate into CHOL-rich microdomains. These data suggest that TNAP penetrates more efficiently and occupies a higher surface area into monolayers with a lower CHOL concentration due to the higher membrane fluidity. However, the quantity of enzyme transferred to solid supports as well as the enzymatic activity were higher using monolayers with a higher CHOL concentration due to increased rigidity that changes the enzyme orientation at the air-solid interface. These data provide new insights regarding the interfacial behavior of TNAP and CHOL in MVs and shed the light on the biochemical and biophysical processes occurring in MV membrane during biomineralization at the molecular level.

[*]*corresponding authors*: massimo.bottini@uniroma2.it, anapr@ffclrp.usp.br.

Graphical Abstract

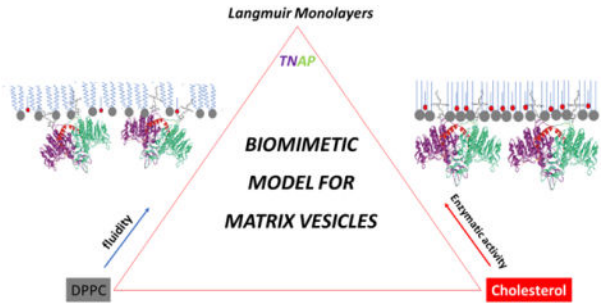

Keywords

Langmuir monolayers; matrix vesicles; cholesterol; alkaline phosphatase; biomimetic models

1. Introduction

Matrix vesicles (MVs) are a special class of extracellular vesicles responsible for the initial deposition of hydroxyapatite (HA) minerals during bone and dentin biomineralization.[1–4] There is experimental evidence that release of MVs occurs at the apical side of microvilli-like membranes of mineral-competent cells, including chondrocytes and osteoblasts since the lipid composition of MVs is very similar to that of apical membranes with a relatively high content of cholesterol (CHOL), phosphatidylserine (PS) and sphingomyelin (SM).[2,4] It has been also shown that MV membrane has a higher concentration of tissue-nonspecific alkaline phosphatase (TNAP) compared to the plasma membrane of parent source cells.[5] TNAP is a phosphohydrolytic enzyme anchored to MV and cell plasma membranes through a glycosylphosphatidylinositol (GPI) anchor. This enzyme participates in the biomineralization processes by hydrolyzing extracellular pyrophosphate (PP_i), a strong mineralization inhibitor, and forming inorganic phosphate (P_i) that enables the growth of mineral crystals inside MVs and their propagation once released in the extracellular matrix.[1,6]

Previous studies have shown that the lipid composition and fluidity of MV membrane modulates the catalytic activity of TNAP and, in turn, affects the deposition of HA minerals during biomineralization.[2,7,8] The molecular structure of the lipids, including the size of the acyl chains and charge of the polar head, influences their distribution on biological membranes due to interactions with fatty acids and/or CHOL and leads to the formation of microdomains with distinct biophysical properties.[9] CHOL is the most abundant and important sterol in human cells. It regulates the organization and fluidity of biological membranes and influences the catalytic activity and incorporation of membrane enzymes.[10,11,12] Bolean *et al.* have shown that the CHOL/phospholipid molar ratio influences the fluidity of liposome membranes and the catalytic activity of membrane-anchored TNAP.[13,14] According to Hanada *et al.*, the strong interactions among sphingolipids, CHOL and GPI-anchored proteins are responsible for the difficulty in removing alkaline phosphatases from biological membranes.[15] Due to the complexity of these structures, membrane models such

as liposomes, proteoliposomes, and lipid Langmuir monolayers are commonly used as biomimetic models for biochemical and biophysical studies of membrane-enzyme interactions.[9,16–21] In particular, the possibility to control the lipid composition and the protein interfacial orientation in two-dimensional Langmuir monolayers makes these structures preferred over liposomes and proteoliposomes when the bilayer structure of the membrane is not the focus of the study.[22] Thus, in the present study we evaluated how CHOL affects both the incorporation of TNAP into dipalmitoylphosphatidylcholine (DPPC)/CHOL Langmuir monolayers and its catalytic activity after incorporation, contributing to the elucidation of the mechanisms driven by TNAP during biomineralization.

2. Materials and Methods

2.1. Materials

1,2-dipalmitoyl-sn-glycero-3-phosphocholine (DPPC; purity > 99%) and 1-palmitoyl-2-{12-[(7-nitro-2–1,3-benzoxadiazol-4-yl)amino]dodecanoyl}-sn-glycero-3-phosphocholine (NBD-PC; purity > 99%) were purchased from Avanti Polar Lipids, Inc. (Alabaster, AL, USA). Chloroform (purity > 99%), Tris (hydroxylmetthyl) aminomethane (Tris; purity ≥ 99.9%), cholesterol (CHOL; purity > 99%), was purchased from Sigma Chemical Co. (St. Louis, MO, USA). Methanol (purity > 99%) was from J.T. Baker (USA). Magnesium chloride and sodium chloride (purity > 99%) was obtained from Synth Co. (Diadema, SP, Brazil). HEPES-buffered saline solution, growth medium (10% fetal calf serum, Dulbecco's modified Eagle's medium) and Calbiosorb resin were used for TNAP expression and purification as described elsewhere[23]. Ultrapure deionized water (resistivity of 18.2 MΩ.cm at 25 °C) from a Milli-Q® system was used in all the experiments.

2.2. Isolation and purification of tissue-nonspecific alkaline phosphatase (TNAP)

TNAP isolation and purification was carried out as previously described by Simão *et al.*[18] Solubilized TNAP was incubated with 200 mg of Calbiosorb resin for 2 h at 4°C under constant stirring in order to remove all non-ionic surfactants and obtain a 0.03 $mg.mL^{-1}$ solution of TNAP in ultrapure deionized water.[24]

2.3. Surface pressure- area (π-A) isotherms

π-A isotherms were recorded at 25.0 ± 0.5°C in a 216 cm^2 Langmuir trough (120 mL) (Insight-Brazil) using ultrapure deionized water as subphase (surface tension 72.8 $mN.m^{-1}$ and resistivity 18.2 MΩ.cm). Table 1 summarizes the features of the Langmuir troughs and the conditions employed for all the experiments. Stock solutions of DPPC and CHOL (1.0 $mmol.L^{-1}$) were prepared in a mixture of chloroform and methanol (3/1, v/v). Lipid solutions were spread at the air/water interface using a microsyringe and the compression was started after 10 min to enable complete solvent evaporation. For enzyme incorporation studies, 5.0 μg of TNAP was injected into the monolayer subphase, which contained 5 $mmol.L^{-1}$ Tris-HCl buffer with 150 $mmol.L^{-1}$ NaCl and 15 $mmol.L^{-1}$ $MgCl_2$ (pH 8.5), leading to a final enzyme concentration of 0.04 $\mu g.mL^{-1}$. The compression was carried out 10 min after enzyme injection.

The compressional modulus (Cs^{-1}) was calculated as:

$$Cs^{-1} = -A\left(\frac{d\pi}{dA}\right)_T \quad \text{(Eq. 1)}$$

Surfactant-free and first-order transition monolayers displayed $Cs^{-1} = 0$. More packed states were reached by increasing monolayer compression, which decreased the lateral compressibility of the monolayer and translates into higher Cs^{-1} values.[25]

2.4. Exclusion pressure (π_{exc}) determination

The incorporation of TNAP into pre-formed monolayers was investigated. The conditions for the formation of the monolayers is depicted in the Table 1. First, the lipid solution was spread at the interface in order to reach a specific value of surface pressure (π_0). Next, 2.5 μg of TNAP was injected in the subphase. The changes in surface pressure ($\Delta\pi$) after the injection of the enzyme were followed and plotted against π_0. The values of π_{exc} were obtained by the extrapolation of the curve to a nil value of $\Delta\pi$.

2.5. Polarization-modulation infrared reflection absorption spectroscopy (PM-IRRAS)

Infrared spectra were recorded at π = 30 mN.m^{-1} in the 800–4000 cm^{-1} range and with a resolution of 8 cm^{-1} by using a KSV PMI550 (*KSV Instruments*) spectrophotometer coupled to a modulation polarizer PEM100. The incident angle was 81°. The characteristics of the Langmuir trough are summarized in the Table 1.

2.6. Fluorescence microscopy (FM) images of the monolayers

Fluorescence micrographs of the monolayers were recorded by using a fluorescence microscopy Olympus BX50 (λ = 390 nm) with a magnification of 40×, coupled to a Langmuir trough (Table 1). Lipid solutions were prepared with 1% mol of fluorescent probe (NBD-PC). The micrographs of pure-lipid monolayers were obtained just before the injection of TNAP into the subphase in order to achieve the best comparisons between the micrographs of the monolayers with and without TNAP.

2.7. Brewster angle microscopy (BAM)

BAM micrographs were recorded using a BAM 2 Plus (Nano Film Technology) coupled to a Langmuir trough (Table 1). A laser with an emission wavelength of 480 nm was used at an angle of 53°. TNAP was injected into the subphase before compression. The monolayers were stable over the time range used in these experiments as observed by the π *vs* time curves (data not shown).

2.8 Transference of the monolayers to solid surfaces: formation of Langmuir-Blodgett (LB) films

A single monolayer containing DPPC:CHOL/TNAP was transferred to a quartz support by means of the LB technique. The support was immersed in the subphase containing 10 mmol.L^{-1} Tris-HCl, 150 mmol.L^{-1} NaCl, 15 mmol.L^{-1} $MgCl_2$ buffer (pH 8.5). Next, the lipid solution was spread at the interface and compressed until π = 30 mN.m^{-1}. Finally, the carrier was moved vertically towards the liquid-air interface at a rate of 0.038 mm.s^{-1} to

obtain a monolayer film with hydrophobic end. The transference was controlled keeping the value of π constant at 30 $mN.m^{-1}$.

The total mass of the lipids and TNAP deposited in the LB films was measured through a Quartz Crystal Microbalance (QCM). The vibration frequency of the piezoelectric crystal is related with the deposited mass by the Sauerbrey equation:

$$\Delta m = -\frac{A\Delta f\sqrt{\rho_q \mu_q}}{2f_0^2} \quad \text{(Eq. 2)}$$

where A is the active piezoelectric area of the crystal, ρ_q is the density of the quartz, μ_q is the quartz shear modulus, f_0 is the vibration frequency of the clean crystal and Δf is the frequency change caused by the deposited mass.[26,27] The quartz crystal used in the present experiment had A = 0.656 cm^2, ρ_q = 2.668 g cm^{-3} and $\mu_q = 2.947\times10^{11}$ $g.cm^{-1}$ s^{-2}.

2.9 Enzymatic kinetics

In order to assess the enzymatic activity of TNAP immobilized in LB films, DPPC:CHOL LB films were transferred to solid supports as described in section 2.8 in presence of the enzyme at the subphase. Next, the supports containing the LB films were immersed in 1.0 mL of a reaction medium composed of an aqueous solution of 70 $mmol.L^{-1}$ of AMPOL pH 10, 10 $mmol.L^{-1}$ of pNPP and 2 $mmol.L^{-1}$ of $MgCl_2$. TNAP catalytic activity of TNAP was monitored by changes in the intensity of the UV-Vis absorption band at 410 nm, corresponding to formation of p-nitrophenolate (pNP^-), a product of enzyme-catalyzed hydrolysis of pNPP. The concentration of pNP^- (molar absorptivity 17600 $mol.L^{-1}.cm^{-1}$) was calculated using Beer's law. The spectra were obtained through a Hewlett Packard model 8453 UV-Vis spectrophotometer. One enzyme unit (U) is defined as the amount of enzyme hydrolyzing 1.0 nmol of substrate per minute at 25°C. The specific catalytic activity of an enzyme is defined as the number of enzyme units per milligram of total protein (U/mg).

3. Results and Discussion

3.1. π-A isotherms

The compressibility of the monolayer was tuned by changing the amount of CHOL in the DPPC monolayer. The π-A isotherms for the pure lipid and mixed monolayers are shown in the Fig. 1. The isotherm for pure DPPC (Fig. 1 – black square) is similar to those found in the literature for this lipid.[28–30] DPPC exhibited an onset π at 95 $Å^2$, corresponding to the beginning of the liquid-expanded (LE) phase, and a plateau of π ~ 10 $mN.m^{-1}$ in the 70–80 $Å^2$ interval, corresponding to the transition from LE to liquid-condensed (LC) phases (coexistence region). The increase of π after this plateau is assigned to region of pure LC phase. The mean molecular area for this lipid was 62 $Å^2$, calculated as the value of the tangent line to the LC phase curve at π=0. The collapse area for pure DPPC was close to 40 $Å^2$ (data not shown) as reported in previous studies.[31,32] On the contrary, CHOL formed condensed monolayers (Fig. 1 – cyan line) and exhibited a mean molecular area close to 42 $Å^2$, similar to those found in the literature.[10,28,30] The incorporation of CHOL into DPPC

monolayers led to the disappearance of the LE/LC coexistence region in the isotherms (Fig 1. circle and triangle) and their gradual shift to lower areas respect to the curve for pure DPPC with increasing the CHOL:DPPC molar ratio. It is worth noting that DPPC:CHOL 4:1 (molar ratio) monolayers showed a mean molecular area of 64 $Å^2$, which was slightly higher than that of DPPC monolayers (62 $Å^2$), suggesting a more expanded monolayer at the LC phase. This result suggests repulsive interactions between the lipids, which may be due to the buffer employed in the subphase (Tris-HCl buffer), since mixtures of DPPC and CHOL form condensed films in pure water[33].

The changes in lipid packing in the monolayers were described by using the Cs^{-1} values calculated from the π-A isotherms. The values of Cs^{-1} reported in Table 2 were obtained at $\pi = 30$ mN.m^{-1}, that is, the value where the thermodynamic parameters of monolayer and bilayer area equalized.[34–36] These values are consistent with the LC state.[25] The high Cs^{-1} value for pure CHOL monolayers can be explained with a high degree of packing of the hydroxyl head groups at the air-water interface, which allows the formation of hydrogen bonds between the sterol molecules.[37] The addition of CHOL to DPPC monolayers had different effects on the Cs^{-1} value in function of the DPPC:CHOL molar ratio. The Cs^{-1} value for DPPC monolayers decreased when 20 mol% of CHOL was added (DPPC:CHOL 4:1 molar ratio), whereas it increased when 50 mol% of CHOL was added (DPPC:CHOL 1:1 molar ratio). In other words, small amounts of CHOL increased the compressional modulus of the DPPC monolayers, while higher amounts of it increased the rigidity, thus suggesting the possibility of controlling the monolayers' rheological parameters by adding different amounts of CHOL. Bolean *et al.* have previously shown that CHOL fluidifies the membranes of binary DPPC:CHOL proteoliposomes.[21] However, the authors observed that an increase in CHOL concentration hampered the incorporation of TNAP into the membrane.

The isotherms of monolayers made of DPPC and CHOL at different molar ratios, both in the presence and absence of TNAP, are depicted in the Fig. 2. The shift of the pure DPPC isotherm to larger areas is due to the ions present in the buffer solution used as a subphase. Sodium and magnesium cations interact with the negative portion of the DPPC phosphatidylcholine group, increasing the net charge of the lipid and leading to more repulsive interactions between the polar heads of the lipids.[38] Slight changes in the pure DPPC isotherm were observed in the presence of TNAP (Fig. 2A). However, an evident area expansion was observed when TNAP was present at the subphase for DPPC:CHOL monolayers. The area expansion was higher for DPPC:CHOL 4:1 (molar ratio) (Fig. 2B) than for DPPC:CHOL 1:1 (molar ratio) monolayer (Fig. 2C). The Fig. 2D compares the values of the area expansion due to TNAP incorporation into the monolayers. This result can be related to the compressibility of the binary DPPC:CHOL monolayers revealed by the Cs^{-1} values described in the Table 2. At lower CHOL molar ratios, the monolayers are more compressible and allow greater enzyme penetration, which translates in a higher area expansion, whereas at a high CHOL molar ratios, the monolayers are less compressible which hampers enzyme penetration. Cs^{-1} values for DPPC, DPPC:CHOL 4:1 and 1:1 (molar ratios) monolayers in the presence of TNAP were 154 ± 7, 140 ± 9 and 171 ± 15 mN.m^{-1}, respectively, which follows the same trend observed in the absence of TNAP (Table 2). However, higher compressional modulus (lower Cs^{-1}) was observed in the

presence of the enzyme, revealing an organizational rearrangement of the monolayer. Similar behavior was also observed in proteoliposomes containing TNAP, DPPC and CHOL.[9]

3.2. Exclusion pressure (π_{exc})

The value of π_{exc} was measured for single component and binary DPPC:CHOL monolayers in order to study the ability of TNAP to penetrate preformed monolayers. The π_{exc} is the surface pressure from which an increase in π is not observed after the addition of the protein, that is, no protein is able to adsorb at the interface.[39,40] In other words, it means that from a lipid packing corresponding to π_{exc} values, TNAP is not able to penetrate the monolayers anymore. Fig. 3 shows the linear dependency between π_0 and $\Delta\pi$ for DPPC, DPPC:CHOL 4:1 and DPPC:CHOL 1:1 (molar ratios) monolayers after the addition of TNAP. The abscissa intercept corresponds to π_{exc}. It was observed that monolayers containing CHOL presented higher $\Delta\pi$ values compared to pure DPPC monolayer. This suggests that, although DPPC:CHOL 1:1 (molar ratio) monolayers exhibited a higher Cs^{-1} value calculated at $\pi=\pi_{exc}$ (Table 3) than pure DPPC monolayers, TNAP penetration was favored by the presence of CHOL, which corroborates the area expansion shown in Fig 2D. Table 3 exhibits the values of π_{exc}. The π_{exc} value for pure DPPC monolayers (12 ± 1 $mN.m^{-1}$) is in agreement with Kouzayha *et al.* (13 $mN.m^{-1}$),[39] which used an alkaline phosphatase isoform from bovine intestine. Higher π_{exc} values were found for DPPC:CHOL 4:1 (molar ratio) monolayers, which suggests a favorable TNAP incorporation compared to the other two types of monolayers.

3.3. Polarization-modulation infrared reflection absorption spectroscopy (PM-IRRAS)

PM-IRRAS spectra of the monolayers were recorded in the 2800–3000 cm^{-1} (Fig. 4A) and 1500–1800 cm^{-1} (Fig. 4B) range of wavelengths, corresponding to C-H stretching mode and amide vibration regions, respectively. The spectra of DPPC monolayers (Fig. 4A and 4B – black lines) are similar to those found in the literature.[41–46] They exhibited the bands corresponding to CH_2 asymmetric stretches at 2920 cm^{-1}, CH_3 stretches at 2880 cm^{-1}, CH_2 symmetric stretches at 2849 cm^{-1}, and C=O ester group stretches at 1728 cm^{-1}. Table 4 describes the assignment of the PM-IRRAS bands. The spectrum of DPPC monolayers containing CHOL (Fig. 4B – blue line) exhibited the band corresponding to R_2C=CHR stretches at 1673 cm^{-1}. The increase in CHOL concentration leads to the shift to lower frequencies of the band assigned to CH_2 asymmetric stretches, which corresponds to the increase of gauche conformers.[47] Additionally, we observe a shift to higher frequencies for the CH_2 symmetric stretch band (Table 4) and the suppression of the CH_3 stretch band in the presence of CHOL. The band corresponding to the carbonyl stretching mode was also shifted in the presence of the sterol. These results suggested that CHOL interacts with both the hydrophobic chains and the polar head group of DPPC. The effects of CHOL on DPPC monolayers have been also investigated by means of vibrational sum frequency generation, which revealed that the condensing effect of CHOL affects the CH_2 stretching region of the spectra[48]. These data are therefore consistent with ours.

Proteins show characteristic PM-IRRAS bands in the 1500–1700 cm^{-1} range of wavelengths, assigned to C=O stretching mode in amides (Amide I) between 1610–1690 cm

$^{-1}$, and to C-N stretching vibrations in combination with N-H bending (Amide II) between 1520–1560 cm^{-1}. Amide I band is more closely related to the protein secondary structure. Antiparallel β-sheets appears at 1630–1640 cm^{-1}, whereas α-helix occurs at 1648–1658 cm^{-1}.[43,49] The TNAP-loaded monolayers exhibited the Amide I band at 1645 cm^{-1}, whereas the Amide II band was observed at 1562 cm^{-1}, thus validating the incorporation of TNAP in the monolayer (Table 4). No β-sheet band was observed, possibly due to the higher amount of α-helix structure in the enzyme (26% of α-helix and 15% of β-sheet).[50] Ronzon *et al.*[40,41,51] studied the incorporation of alkaline phosphatase from bovine intestine in DPPC monolayers using PM-IRRAS. The authors observed the Amide I band at 1646 and 1633 cm^{-1} (α-helix and β-sheet, respectively), and the Amide II at 1540 cm^{-1}. However, the intestinal isoform is only 50% similar to TNAP, which gives rise to the observed difference between these results and ours.[50,52] The band at 1678 cm^{-1} (Fig. 5B – red line) can be assigned to turns in the protein structure.[49] Caseli *et al.*[53] solubilized rat osseous plate alkaline phosphatase with polidocanol and found that the bands assigned to the amide groups were centered at approximately 1653, 1620 and 1539 cm^{-1} when the enzyme was spread purely both on the buffer-air interface and in presence of a negatively charged phospholipid. The presence of β-sheet bands, and the fact of the amide II had higher intensity than the amide I bands, differently from what was presented in our case, overall suggests that the enzyme secondary structure, as well as the orientation of the enzyme at the interface, is driven by the microenvironment available for the alkaline phosphatase at the air-water interface. The conservation of the secondary structure of the enzyme was expected since the GPI anchor can drive the incorporation of the enzyme in the monolayer, with the hydrophilic moieties turned towards the aqueous phase.

The incorporation of TNAP led to a shift of both CH_2 asymmetric and carbonyl bands (Table 4), suggesting interactions between the enzyme and both the hydrophobic chains and the polar head group of DPPC. For the DPPC:CHOL 4:1 mixture, both CH_2 and carbonyl bands were shifted, whereas no CH_2 band shift was observed for the 1:1 ratio mixed monolayer. Due to the higher compressional modulus of DPPC:CHOL 4:1 (molar ratio) monolayers, a higher and deeper penetration is probable, leading to interactions between DPPC acyl chains and the enzyme. Instead, the rigid monolayer formed by DPPC and CHOL at a molar ratio of 1:1 restricts the TNAP penetration, enabling the interactions with only DPPC head group. By using computational chemistry, Cornut *et al.*[54] observed a negative orientation with respect to the baseline for α-helix Amide I bands oriented at angles lower than 45° to the surface. Additionally, they observed that the angle of helix inclination increases with the ratio between the Amide I and Amide II intensities. The spectrum in Fig. 4B (red line) suggests that the ellipsoidal polypeptide structure of the enzyme presented an orientation between 45° and 90° when anchored to the DPPC monolayer. Small differences between Amide I and Amide II bands were observed, indicating that CHOL influences the conformation and orientation of TNAP on DPPC monolayers. This translates in changes in the catalytic activity of TNAP in presence of CHOL. Recently, Favarin *et al.*[7] observed that the presence of sterols in DPPC proteoliposomes influences the kinetic parameters of TNAP due to changes in the organization of the membrane. Our PM-IRRAS results showed that the compressibility of the membrane leads to bending of the GPI acyl chains of the enzyme, which translated into different orientation of the globular portion of the protein with respect

to the lipid interface compared to rigid DPPC membranes. Such greater freedom degree of the anchor protein causes conformational changes in the globular structure of the TNAP, thus leading to significant changes in the catalytic properties of the enzyme as described in previous studies.[7,18,26,55–57]

3.4. Fluorescence microscopy (FM)

FM micrographs of DPPC and DPPC:CHOL monolayers in the presence and absence of TNAP are shown in Fig. 5. Light regions are assigned to DPPC-rich domains, while dark regions are consistent with the absence of the lipid. The dark regions at π = 15 mN.m^{-1} are defects in the DPPC monolayer (Fig. 5A), which were not observed at π = 30 mN.m^{-1}, indicating a homogeneous LC phase. The dark regions in Fig. 5B indicate phase segregation between DPPC and CHOL due to their electrostatic interactions. Stottrup *et al.*[11] described that two different regions occurs in DPPC:CHOL mixed monolayers, depending on the composition of the monolayers. Alpha-regions occurs at CHOL concentrations lower than 40 mol% and are characterized by dark domains on a light background, whereas β-regions occur at higher CHOL concentrations and are characterized by light domains on a dark background. These behaviors were observed in the micrographs presented in the Fig. 5.

The injection of TNAP into the subphase resulted in morphological changes in the monolayers, evidencing the incorporation of the enzyme (Figs. 5D, 5E and 5F). Enzyme incorporation even at π values greater than the π_{exc} (Table 3) indicates that the protein penetrates entirely in the monolayer at π values smaller than π_{exc}, whereas only the GPI acyl chains inserted in the monolayer at π values greater than π_{exc} as suggested by Caseli *et al.*[58] for the incorporation of detergent-solubilized alkaline phosphatase into negatively charged phospholipids monolayers. The similarity between the double-carbonic chain of DPPC and TNAP GPI acyl chains, as well as the low amount of TNAP molecules compared to DPPC, are responsible for the discrete π changes. The presence of TNAP led to a more uniform distribution and an increase in the size of CHOL-rich domains, indicating the preferential incorporation of the enzyme in these monolayer regions. This fact is evidenced by Figs. 5D and 5E at π = 30 mN.m^{-1}, where elongated and amorphous 5 μm-in-size domains were observed for DPPC monolayers, while well-defined 20 μm-in-size domains were observed for DPPC:CHOL 4:1 (molar ratio) monolayers. These results corroborate the previous hypothesis about the favorable interactions between the GPI-anchor and CHOL molecules.

3.5. Brewster angle microscopy (BAM)

BAM micrographs of the monolayers for several π values are shown in Fig. 6. Light regions correspond to LC phase domains, while dark regions correspond to LE phase or absence of amphiphilic molecules. The existence of LC phase at low π can be assigned to elevated compression rates.[59] For DPPC, the initial compression led to domain nucleation, thus resulting in a homogeneous LC phase at π = 30 mN.m^{-1}. The presence of TNAP increased the size of the LE domains, validating its incorporation. The existence of LE phase explains the increase in compressibility due to the presence of TNAP. Kouzayha and Besson[39] obtained similar results for alkaline phosphatase from bovine intestine on DPPC

monolayers. The increased compressibility resulted in reduction of the phase transition enthalpy, but does not alter the transition temperature as reported by Bolean *et al.*[13]

Differences in the BAM images assigned to the presence of TNAP in the CHOL-containing monolayers were evident only at π=1 mN.m^{-1}. Homogeneously distributed LE domains were observed in the presence of TNAP, validating the incorporation of the enzyme even at low π values. Guzmán *et al.*[28] described that CHOL disperses between DPPC molecules to avoid the contact of its hydrophobic rings with water, leading to monolayer reorganization and preventing the nucleation of DPPC domains. This behavior makes difficult to observe any difference between the monolayers at higher values of π.

3.6. Langmuir-Blodgett films: transfer of TNAP to solid supports

The amount of lipids and protein transferred to solid supports was determined by QCM (Table 5). The results reveal that a greater amount of protein was observed for the monolayer with increased CHOL content although the DPPC:CHOL 4:1 (molar ratio) mixture favors the penetration of TNAP into DPPC monolayers as evidenced by higher area expansion (Fig. 2D). This result can be related to the higher compressibility of the DPPC:CHOL (4:1) compared to DPPC:CHOL (1:1), which hampers the transfer from the liquid-air to the solid-air interface.

The specific catalytic activity of TNAP immobilized in Langmuir-Blodgett films was also assessed (Table 5). Once more, increased enzymatic activity was observed for the more rigid monolayers made of pure DPPC and DPPC:CHOL 1:1 although greater enzyme penetration was favored into more compressible monolayers, that is, DPPC:CHOL 4:1 mixtures exhibiting a more favorable TNAP incorporation compared to the other two types of monolayers studied (Fig. 3 and Table 3). Since the values of Cs^{-1} for these monolayers are comparable (154 ± 7 and 171 ± 15 mN.m^{-1}, respectively), the increased amount of TNAP transferred to DPCC:CHOL 1:1 can be assigned to the higher affinity of the enzyme to CHOL. This result is also corroborated by the PM-IRRAS data: the enzyme penetrates the monolayer by its GPI-anchor at higher amounts of CHOL thus exposing better the catalytic site to the media, as depicted in the schematic representation shown in Fig. 7.

4. Conclusion

In this study, the effect of CHOL on the incorporation of TNAP into DPPC monolayers was investigated by using Langmuir monolayers as membrane biomimetic systems. Data on π-A isotherms and Cs^{-1} for binary DPPC:CHOL monolayers revealed that CHOL plays a role in the compressibility of the membrane and affects TNAP incorporation. TNAP incorporation was favored at lower CHOL concentrations due to the fluidized monolayer. Instead, higher CHOL concentrations decreased TNAP incorporation due to the formation of a more rigid monolayer. This behavior was reflected in the π_{exc} data: greater values of π_{exc} were found for DPPC:CHOL (4:1) molar ratio, the most compressible monolayer, and assigned to a higher enzyme penetration. PM-IRRAS spectra not only validated TNAP incorporation in all the monolayers studied, but confirmed the partial maintenance of its secondary structure and revealed that the packing and compressibility of the monolayer are disturbed upon enzyme incorporation. It was also shown that the conformation and/or orientation of the enzyme are

modulated by the presence and concentration of CHOL. FM and BAM micrographs revealed that the composition of the monolayer influences LC/LE domains formation. The incorporation of TNAP was confirmed by the appearance of circular and homogeneously distributed domains. CHOL concentration influenced the dimension of TNAP-rich domains: higher CHOL concentrations led to bigger domains, indicating the preferential incorporation of the enzyme. Taken together, these results showed that both TNAP incorporation and catalytic activity are modulated by membrane fluidity, driven by the presence of CHOL, providing support to better understand the interfacial behavior between CHOL and TNAP in MV membrane and helping to clarify complex biochemical and biophysical processes that occur in MV membrane during biomineralization.

Acknowledgements

This study was supported by the Sao Paulo Research Foundation (FAPESP grants 2015/03594-4; 2014/11941-3; 2016/21236-0; 2017/08892-9), Coordination for the Improvement of Higher Education Personnel (CAPES) - Finance Code 001 and by the Brazilian National Council of Technological and Scientific Development (CNPq grants 442834/2014-4; 304021/2017-2; 167497/2017-0). This project was also supported by the project NanOArt from the University of Rome Tor Vergata. PC, APR, and LC are researcher of CNPq. The authors thank Prof. Osvaldo Novais de Oliveira Junior for the accesses to BAM and PM-IRRAS facilities.

References

(1). Clarke Anderson H, Rama Garimella SET The Role of Matrix Vesicles in Growth Plate Development and Biomineralization. Front. Biosci 2005, 10, 822–837. [PubMed: 15569622]

(2). Bottini M; Mebarek S; Anderson KL; Strzelecka-Kiliszek A; Bozycki L; Simão AMS; Bolean M; Ciancaglini P; Pikula JB; Pikula S; et al. Matrix Vesicles from Chondrocytes and Osteoblasts: Their Biogenesis, Properties, Functions and Biomimetic Models. Biochim. Biophys. Acta - Gen. Subj 2018, 1862 (3), 532–546. 10.1016/j.bbagen.2017.11.005. [PubMed: 29108957]

(3). Wuthier RE Matrix Vesicles: Structure, Composition, Formation and Function in Calcification. Front. Biosci 2011, 16 (1), 2812 10.2741/3887.

(4). Plaut JS; Strzelecka-Kiliszek A; Bozycki L; Pikula S; Buchet R; Mebarek S; Chadli M; Bolean M; Simao AMS; Ciancaglini P; et al. Quantitative Atomic Force Microscopy Provides New Insight into Matrix Vesicle Mineralization. Arch. Biochem. Biophys 2019, 667, 14–21. 10.1016/j.abb.2019.04.003. [PubMed: 30998909]

(5). Thouverey C; Strzelecka-Kiliszek A; Balcerzak M; Buchet R; Pikula S Matrix Vesicles Originate from Apical Membrane Microvilli of Mineralizing Osteoblast-like Saos-2 Cells. J. Cell. Biochem 2009, 106 (1), 127–138. 10.1002/jcb.21992. [PubMed: 19009559]

(6). Cui L; Houston DA; Farquharson C; MacRae VE Characterisation of Matrix Vesicles in Skeletal and Soft Tissue Mineralisation. Bone 2016, 87, 147–158. 10.1016/j.bone.2016.04.007. [PubMed: 27072517]

(7). Favarin BZ; Andrade MAR; Bolean M; Simão AMS; Ramos AP; Hoylaerts MF; Millán JL; Ciancaglini P Effect of the Presence of Cholesterol in the Interfacial Microenvironment on the Modulation of the Alkaline Phosphatase Activity during in Vitro Mineralization. Colloids Surfaces B Biointerfaces 2017, 155, 466–476. 10.1016/j.colsurfb.2017.04.051. [PubMed: 28472750]

(8). Simão AMS; Bolean M; Favarin BZ; Veschi EA; Tovani CB; Ramos AP; Bottini M; Buchet R; Millán JL; Ciancaglini P Lipid Microenvironment Affects the Ability of Proteoliposomes Harboring TNAP to Induce Mineralization without Nucleators. J. Bone Miner. Metab 2019, 37 (4), 607–613. 10.1007/s00774-018-0962-8. [PubMed: 30324534]

(9). Bolean M; Simão AMS; Favarin BZ; Millán JL; Ciancaglini P Thermodynamic Properties and Characterization of Proteoliposomes Rich in Microdomains Carrying Alkaline Phosphatase. Biophys. Chem 2011, 158 (2–3), 111–118. 10.1016/j.bpc.2011.05.019. [PubMed: 21676530]

(10). Wydro P The Influence of Cholesterol on Multicomponent Langmuir Monolayers Imitating Outer and Inner Leaflet of Human Erythrocyte Membrane. Colloids Surfaces B Biointerfaces 2013, 103, 67–74. 10.1016/j.colsurfb.2012.10.020. [PubMed: 23201721]

(11). Stottrup BL; Keller SL Phase Behavior of Lipid Monolayers Containing DPPC and Cholesterol Analogs. Biophys. J 2006, 90 (9), 3176–3183. 10.1529/biophysj.105.072959. [PubMed: 16461392]

(12). Kim K; Kim C; Byun Y Preparation of a Dipalmitoylphosphatidylcholine/Cholesterol Langmuir-Blodgett Monolayer That Suppresses Protein Adsorption. Langmuir 2001, 17 (16), 5066–5070. 10.1021/la0102096.

(13). Bolean M; Simão a M. S.; Favarin BZ; Millán JL; Ciancaglini P Thermodynamic Properties and Characterization of Proteoliposomes Rich in Microdomains Carrying Alkaline Phosphatase. Biophys. Chem 2011, 158 (2–3), 111–118. 10.1016/j.bpc.2011.05.019. [PubMed: 21676530]

(14). Bolean M; Simão AMS; Favarin BZ; Millán JL; Ciancaglini P The Effect of Cholesterol on the Reconstitution of Alkaline Phosphatase into Liposomes. Biophys. Chem 2010, 152 (1–3), 74–79. 10.1016/j.bpc.2010.08.002. [PubMed: 20810204]

(15). Hanada K; Nishijima M; Akamatsu Y; Pagano RE Both Sphingolipids and Cholesterol Participate in the Detergent Insolubility of Alkaline Phosphatase, a Glycosylphosphatidylinositol-Anchored Protein, in Mammalian Membranes. J. Biol. Chem 1995, 270 (11), 6254–6260. 10.1074/jbc.270.11.6254. [PubMed: 7890763]

(16). Bolean M; Borin IA; Simão AMS; Bottini M; Bagatolli LA; Hoylaerts MF; Millán JL; Ciancaglini P Topographic Analysis by Atomic Force Microscopy of Proteoliposomes Matrix Vesicle Mimetics Harboring TNAP and AnxA5. Biochim. Biophys. Acta - Biomembr 2017, 1859 (10), 1911–1920. 10.1016/j.bbamem.2017.05.010. [PubMed: 28549727]

(17). Bolean M; Simão AMS; Barioni MB; Favarin BZ; Sebinelli HG; Veschi EA; Janku TAB; Bottini M; Hoylaerts MF; Itri R; et al. Biophysical Aspects of Biomineralization. Biophys. Rev 2017, 9 (5), 747–760. 10.1007/s12551-017-0315-1. [PubMed: 28852989]

(18). Simão AMS; Yadav MC; Narisawa S; Bolean M; Pizauro JM; Hoylaerts MF; Ciancaglini P; Luis Milla J Proteoliposomes Harboring Alkaline Phosphatase and Nucleotide Pyrophosphatase as Matrix Vesicle Biomimetics. J. Biol. Chem 2010, 285 (10), 7598–7609. 10.1074/jbc.M109.079830. [PubMed: 20048161]

(19). Ciancaglini P; Simão a. M. S.; Bolean M; Millán JL; Rigos CF; Yoneda JS; Colhone MC; Stabeli RG Proteoliposomes in Nanobiotechnology. Biophys. Rev 2012, 4 (1), 67–81. 10.1007/s12551-011-0065-4. [PubMed: 28510001]

(20). Morandat S; Bortolato M; Roux B Cholesterol-Dependent Insertion of Glycosylphosphatidylinositol-Anchored Enzyme. Biochim. Biophys. Acta - Biomembr 2002, 1564 (2), 473–478. 10.1016/S0005-2736(02)00497-2.

(21). Bolean M; Simão a. M. S.; Favarin BZ; Millán JL; Ciancaglini P The Effect of Cholesterol on the Reconstitution of Alkaline Phosphatase into Liposomes. Biophys. Chem 2010, 152 (1–3), 74–79. 10.1016/j.bpc.2010.08.002. [PubMed: 20810204]

(22). Brockman H Lipid Monolayers : Why Use Half a Membrane Interactions to Characterize Protein-Membrane Interactions? Curr. Opin. Stru 1999, 9, 438–443.

(23). Simão AMS; Beloti MM; Cezarino RM; Rosa AL; Pizauro JM; Ciancaglini P Membrane-Bound Alkaline Phosphatase from Ectopic Mineralization and Rat Bone Marrow Cell Culture. Comp. Biochem. Physiol. A. Mol. Integr. Physiol 2007, 146 (4), 679–687. 10.1016/j.cbpa.2006.05.008. [PubMed: 16798036]

(24). Camolezi FL; Daghastanli KRP; Magalhães PP; Pizauro JM; Ciancaglini P Construction of an Alkaline Phosphatase-Liposome System: A Tool for Biomineralization Study. Int. J. Biochem. Cell Biol 2002, 34 (9), 1091–1101. 10.1016/S1357-2725(02)00029-8. [PubMed: 12009304]

(25). Vollhardt D; Fainerman VB Progress in Characterization of Langmuir Monolayers by Consideration of Compressibility. Adv. Colloid Interface Sci 2006, 127 (2), 83–97. 10.1016/j.cis.2006.11.006. [PubMed: 17208192]

(26). Caseli L; Furriel RPM; de Andrade JF; Leone FA; Zaniquelli MED Surface Density as a Significant Parameter for the Enzymatic Activity of Two Forms of Alkaline Phosphatase

Immobilized on Phospholipid Langmuir-Blodgett Films. J. Colloid Interface Sci 2004, 275 (1), 123–130. [PubMed: 15158389]

(27). Wang M; Zander T; Liu X; Liu C; Raj A; Florian Wieland DC; Garamus VM; Willumeit-Römer R; Claesson PM; Dėdinaitė A The Effect of Temperature on Supported Dipalmitoylphosphatidylcholine (DPPC) Bilayers: Structure and Lubrication Performance. J. Colloid Interface Sci 2015, 445, 84–92. 10.1016/j.jcis.2014.12.042. [PubMed: 25596372]

(28). Guzmán E; Liggieri L; Santini E; Ferrari M; Ravera F Mixed DPPC-Cholesterol Langmuir Monolayers in Presence of Hydrophilic Silica Nanoparticles. Colloids Surfaces B Biointerfaces 2013, 105, 284–293. 10.1016/j.colsurfb.2013.01.020. [PubMed: 23384691]

(29). Torrano A. a.; Pereira ÂS; Oliveira ON; Barros-Timmons A Probing the Interaction of Oppositely Charged Gold Nanoparticles with DPPG and DPPC Langmuir Monolayers as Cell Membrane Models. Colloids Surfaces B Biointerfaces 2013, 108, 120–126. 10.1016/j.colsurfb.2013.02.014. [PubMed: 23528608]

(30). Jurak M; Golabek M; Holysz L; Chibowski E Properties of Langmuir and Solid Supported Lipid Films with Sphingomyelin. Adv. Colloid Interface Sci 2014, 1–13. 10.1016/j.cis.2014.03.008.

(31). Albrecht O; Gruler H; Sackmann E Pressure-Composition Phase Diagrams of Cholesterol/ Lecithin, Cholesterol/Phosphatidic Acid, and Lecithin/Phosphatidic Acid Mixed Monolayers: A Langmuir Film Balance Study. J. Colloid Interface Sci 1981, 79 (2), 319–338. 10.1007/978-3-642-51881-2.

(32). Ma G; Allen HC DPPC Langmuir Monolayer at the Air−Water Interface: Probing the Tail and Head Groups by Vibrational Sum Frequency Generation Spectroscopy. Langmuir 2006, 22 (12), 5341–5349. 10.1021/la0535227. [PubMed: 16732662]

(33). Sugawara A; Nishimura T; Yamamoto Y; Inoue H; Nagasawa H; Kato T Self-Organization of Oriented Calcium Carbonate/Polymer Composites: Effects of a Matrix Peptide Isolated from the Exoskeleton of a Crayfish. Angew. Chem. Int. Ed. Engl 2006, 45 (18), 2876–2879. 10.1002/ anie.200503800. [PubMed: 16550616]

(34). Seelig A Local Anesthetics and Pressure: A Comparison of Dibucaine Binding to Lipid Monolayers and Bilayers. BBA - Biomembr 1987, 899 (2), 196–204. 10.1016/0005-2736(87)90400-7.

(35). Blume A A Comparative Study of the Phase Transitions of Phospholipid Bilayers and Monolayers. BBA - Biomembr 1979, 557 (1), 32–44. 10.1016/0005-2736(79)90087-7.

(36). Marsh D Lateral Pressure in Membranes. Biochim. Biophys. Acta - Rev. Biomembr 1996, 1286 (3), 183–223. 10.1016/S0304-4157(96)00009-3.

(37). Lintker KB; Kpere-Daibo P; Fliesler SJ; Serfis AB A Comparison of the Packing Behavior of Egg Phosphatidylcholine with Cholesterol and Biogenically Related Sterols in Langmuir Monolayer Films. Chem. Phys. Lipids 2009, 161 (1), 22–31. 10.1016/ j.chemphyslip.2009.06.139. [PubMed: 19524563]

(38). Lee Y-L; Lin J-Y; Chang C-H Thermodynamic Characteristics and Langmuir-Blodgett Deposition Behavior of Mixed DPPA/DPPC Monolayers at Air/Liquid Interfaces. J. Colloid Interface Sci 2006, 296 (2), 647–654. 10.1016/j.jcis.2005.09.050. [PubMed: 16225885]

(39). Kouzayha A; Besson F GPI-Alkaline Phosphatase Insertion into Phosphatidylcholine Monolayers: Phase Behavior and Morphology Changes. Biochem. Biophys. Res. Commun 2005, 333 (4), 1315–1321. 10.1016/j.bbrc.2005.06.049. [PubMed: 15979580]

(40). Ronzon F; Desbat B; Chauvet JP; Roux B Penetration of a GPI-Anchored Protein into Phospholipid Monolayers Spread at the Air/Water Interface. Colloids Surfaces B Biointerfaces 2002, 23 (4), 365–373. 10.1016/S0927-7765(01)00271-5.

(41). Ronzon F; Desbat B; Chauvet JP; Roux B Behavior of a GPI-Anchored Protein in Phospholipid Monolayers at the Air-Water Interface. Biochim. Biophys. Acta - Biomembr 2002, 1560 (1–2), 1–13. 10.1016/S0005-2736(01)00405-9.

(42). He Q; Li J Hydrolysis Characterization of Phospholipid Monolayers Catalyzed by Different Phospholipases at the Air-Water Interface. Adv. Colloid Interface Sci 2007, 131 (1–2), 91–98. 10.1016/j.cis.2006.11.002. [PubMed: 17210114]

(43). Mendelsohn Richard, Mao Guangru, and F CR. Infrared Reflection-Absorption Spectroscopy: Principles and Applications to Lipid-Protein Interaction in Langmuir Films. Biochim Biophys Acta 2010, 1798 (5), 788–800. 10.1016/j.immuni.2010.12.017.Two-stage. [PubMed: 20004639]

(44). Mendelsohn R; Flach CR Infrared Reflection–Absorption Spectrometry of Monolayer Films at the Air–Water Interface. Handb. Vib. Spectrosc 2002, No. 2, 1028–1041. 10.1146/annurev.pc.46.100195.001513.

(45). Mendelsohn R; Flach CR Handbook of Vibrational Spectroscopy. Vol II - Infrared Reflection – Absorption Spectrometry of Monolayer Films at the Air – Water Interface; Wiley: Rutgers University, Newark, NJ, USA, 2002.

(46). Pavinatto A; Delezuk JAM; Souza AL; Pavinatto FJ; Volpati D; Miranda PB; Campana-Filho SP; Oliveira ON Experimental Evidence for the Mode of Action Based on Electrostatic and Hydrophobic Forces to Explain Interaction between Chitosans and Phospholipid Langmuir Monolayers. Colloids Surfaces B Biointerfaces 2016, 145 (June), 201–207. 10.1016/j.colsurfb.2016.05.001. [PubMed: 27182655]

(47). Ren Y; Kato T Polarized Infrared External Reflection Spectroscopy of a Uniaxial Monolayer at the Air/Water Interface. Langmuir 2002, 18 (17), 6699–6705. 10.1021/la020185i.

(48). Bonn M; Roke S; Berg O; Juurlink LBF; Stamouli A; Müller M A Molecular View of Cholesterol-Induced Condensation in a Lipid Monolayer. J. Phys. Chem. B 2004, 108 (50), 19083–19085. 10.1021/jp0452249.

(49). Barth A; Zscherp C What Vibrations Tell about Proteins. Q. Rev. Biophys 2002, 35 (4), 369–430. 10.1017/S0033583502003815. [PubMed: 12621861]

(50). Le Du M-H Structural Evidence of Functional Divergence in Human Alkaline Phosphatases. J. Biol. Chem 2002, 277 (51), 49808–49814. 10.1074/jbc.M207394200. [PubMed: 12372831]

(51). Ronzon F; Desbat B; Buffeteau T; Mingotaud C; Chauvet JP; Roux B Structure and Orientation of a Glycosylphosphatidyl Inositol Anchored Protein at the Air/Water Interface. J. Phys. Chem. B 2002, 106 (12), 3307–3315. 10.1021/jp0119983.

(52). Estaki M; DeCoffe D; Gibson DL Interplay between Intestinal Alkaline Phosphatase, Diet, Gut Microbes and Immunity. World J. Gastroenterol 2014, 20 (42), 15650–15656. 10.3748/wjg.v20.i42.15650. [PubMed: 25400448]

(53). Caseli L; Masui DC; Furriel RPM; Leone FA; Zaniquelli MED; Orbulescu J; Leblanc RM Rat Osseous Plate Alkaline Phosphatase as Langmuir Monolayer—An Infrared Study at the Air–Water Interface. J. Colloid Interface Sci 2008, 320 (2), 476–482. 10.1016/j.jcis.2008.01.043. [PubMed: 18280491]

(54). Cornut I; Desbat B; Turlet JM; Dufourcq J In Situ Study by Polarization Modulated Fourier Transform Infrared Spectroscopy of the Structure and Orientation of Lipids and Amphipathic Peptides at the Air-Water Interface. Biophys. J 1996, 70 (1), 305–312. 10.1016/S0006-3495(96)79571-1. [PubMed: 8770206]

(55). Andrade MAR; Favarin B; Derradi R; Bolean M; Simão AMS; Millán JL; Ciancaglini P; Ramos AP Pendant-Drop Method Coupled to Ultraviolet-Visible Spectroscopy : A Useful Tool to Investigate Interfacial Phenomena. Colloids Surfaces A Physicochem. Eng. Asp 2016, 504, 305–311. 10.1016/j.colsurfa.2016.05.085.

(56). Andrade MAR; Derradi R; Simão AMS; Millán JL; Ramos AP; Ciancaglini P; Bolean M Is Alkaline Phosphatase Biomimeticaly Immobilized on Titanium Able to Propagate the Biomineralization Process? Arch. Biochem. Biophys 2019, 663 (January), 192–198. 10.1016/j.abb.2019.01.014. [PubMed: 30659801]

(57). Bolean M; Simão AMS; Kiffer-Moreira T; Hoylaerts MF; Millán JL; Itri R; Ciancaglini P Proteoliposomes with the Ability to Transport Ca^{2+} into the Vesicles and Hydrolyze Phosphosubstrates on Their Surface. Arch. Biochem. Biophys 2015, 584, 79–89. 10.1016/j.abb.2015.08.018. [PubMed: 26325078]

(58). Caseli L; Masui DC; Furriel RPM; Leone FA; Zaniquelli MED Incorporation Conditions Guiding the Aggregation of a Glycosylphosphatidyl Inositol (GPI) -Anchored Protein in Langmuir Monolayers. Colloids Surfaces B Biointerfaces 2005, 46, 248–254. 10.1016/j.colsurfb.2005.11.007. [PubMed: 16356698]

(59). Gehlert U; Vollhardt D Nonequilibrium Structures in 1-Monopalmitoyl-Roc-Glycerol Monolayers. Langmuir 1997, 13 (2), 277–282.

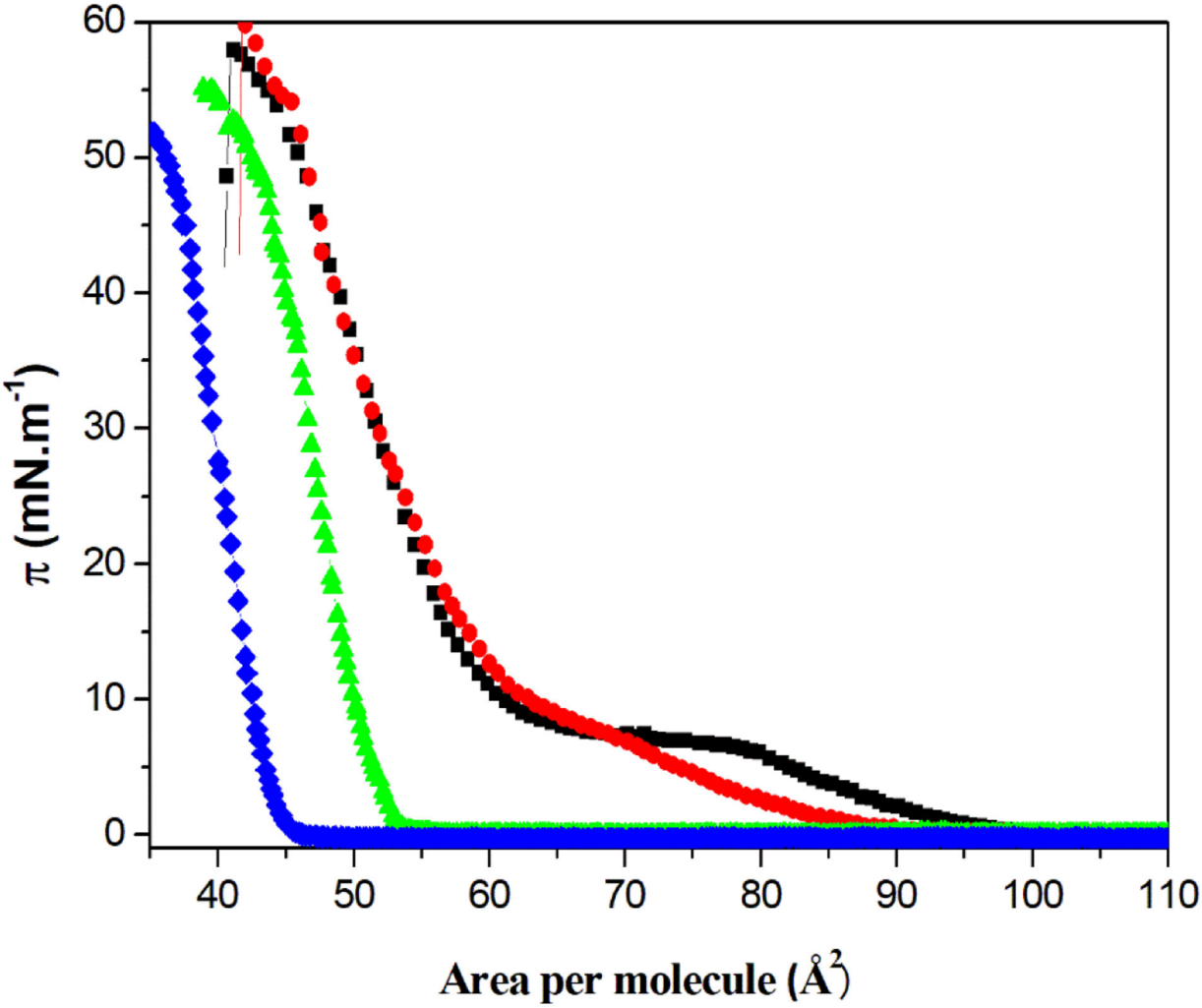

Fig. 1.

π–A isotherms of the single component DPPC and binary DPPC:CHOL (molar ratios) monolayers, at the air-water interface. Pure DPPC (■), DPPC:CHOL 4:1 (●), DPPC:CHOL 1:1 (▲), and pure CHOL (♦).

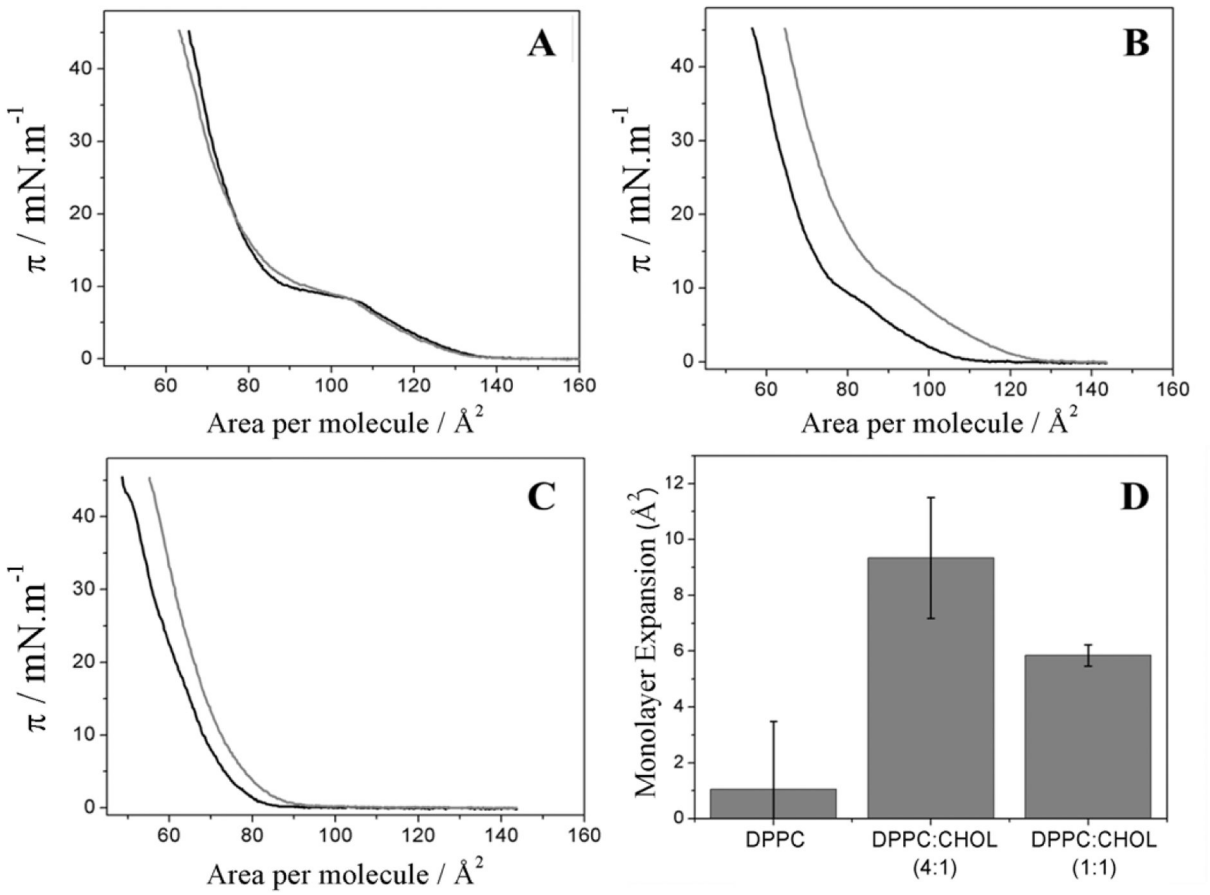

Fig. 2.

π–A isotherms of the monolayers containing DPPC **(A)**, DPPC:CHOL 4:1 **(B)**, and DPPC:CHOL 1:1 **(C)** (molar ratios) with (grey lines) and without (black lines) TNAP on subphase of 5 mmol.L^{-1} Tris-HCl buffer with 150 mmol.L^{-1} NaCl and 15 mmol.L^{-1} $MgCl_2$ (pH 8.5), and the comparison between the area expansion at **π** = 30 mN.m^{-1} due to TNAP penetration **(D)**.

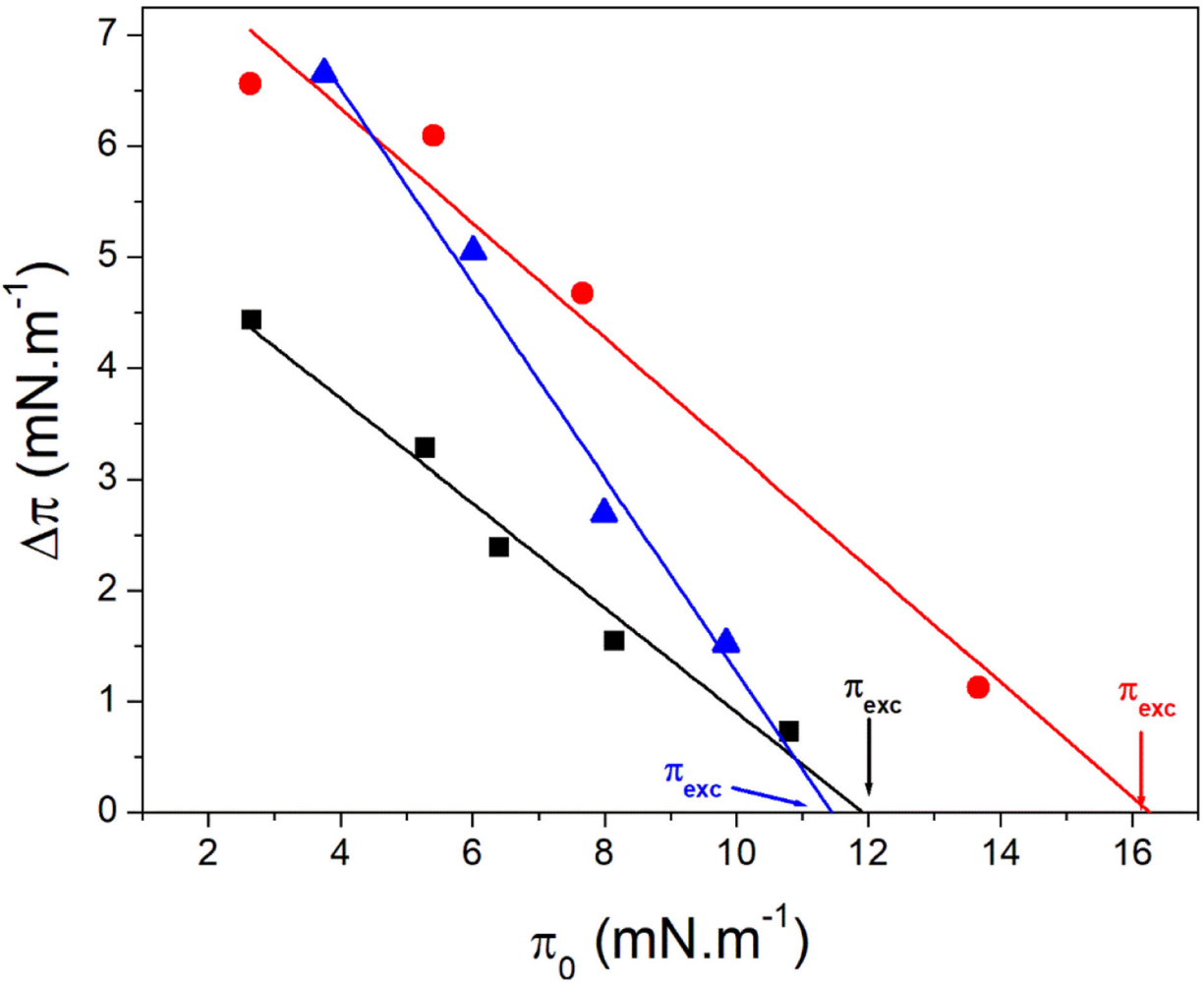

Fig. 3.

Changes in the surface pressure ($\Delta\pi$) *vs* the initial surface pressure (π_0) for DPPC (■), DPPC:CHOL 4:1 (●) and DPPC:CHOL 1:1 (▲) monolayers due to injection of TNAP at subphase. The intercept with abscissa indicated by the arrows is the π_{exc}.

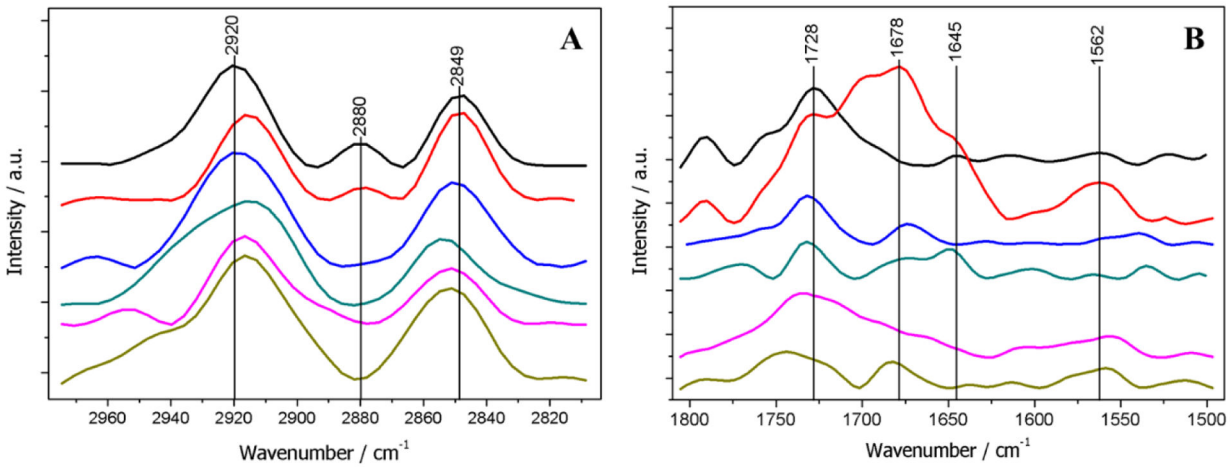

Fig. 4.

PM-IRRAS spectra of mixed monolayers at π = 30 mN.m^{-1}, obtained from 2800–3000 cm^{-1} **(A)** and 1500–1800 cm^{-1} **(B)**, corresponding to C-H and amide stretches, respectively. DPPC (black line); DPPC + TNAP (red line); DPPC:CHOL 4:1 (blue line); DPPC:CHOL 4:1 + TNAP (green line); DPPC:CHOL 1:1 (pink line); DPPC:CHOL 1:1 + TNAP (dark yellow line).

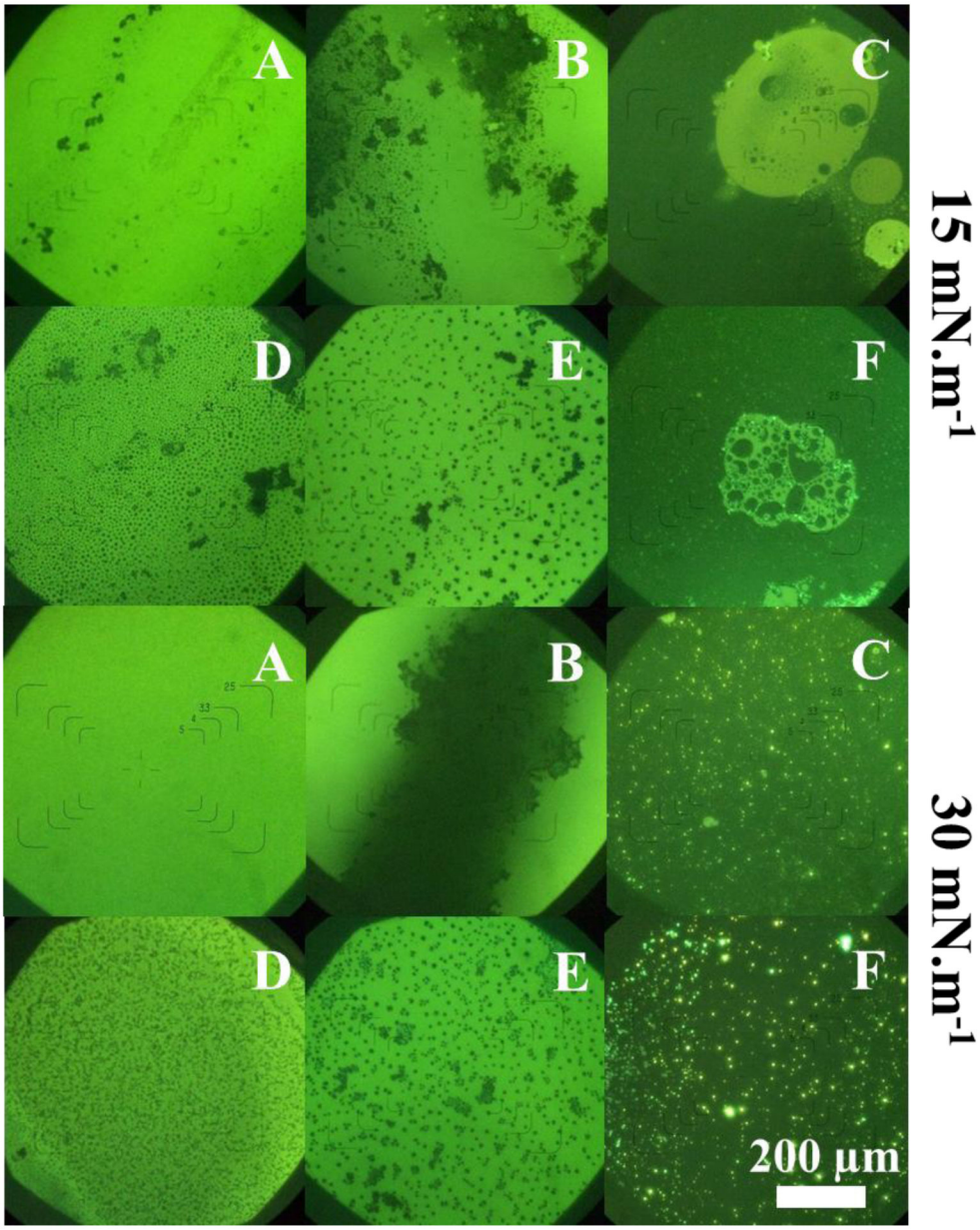

Fig. 5.

FM micrographs at π = 15 mN.m^{-1} and π = 30 mN.m^{-1}. **(A)** DPPC; **(B)** DPPC:CHOL 4:1; **(C)** DPPC:CHOL 1:1; **(D)** DPPC + TNAP; **(E)** DPPC:CHOL 4:1 + TNAP; **(F)** DPPC:CHOL 1:1 + TNAP.

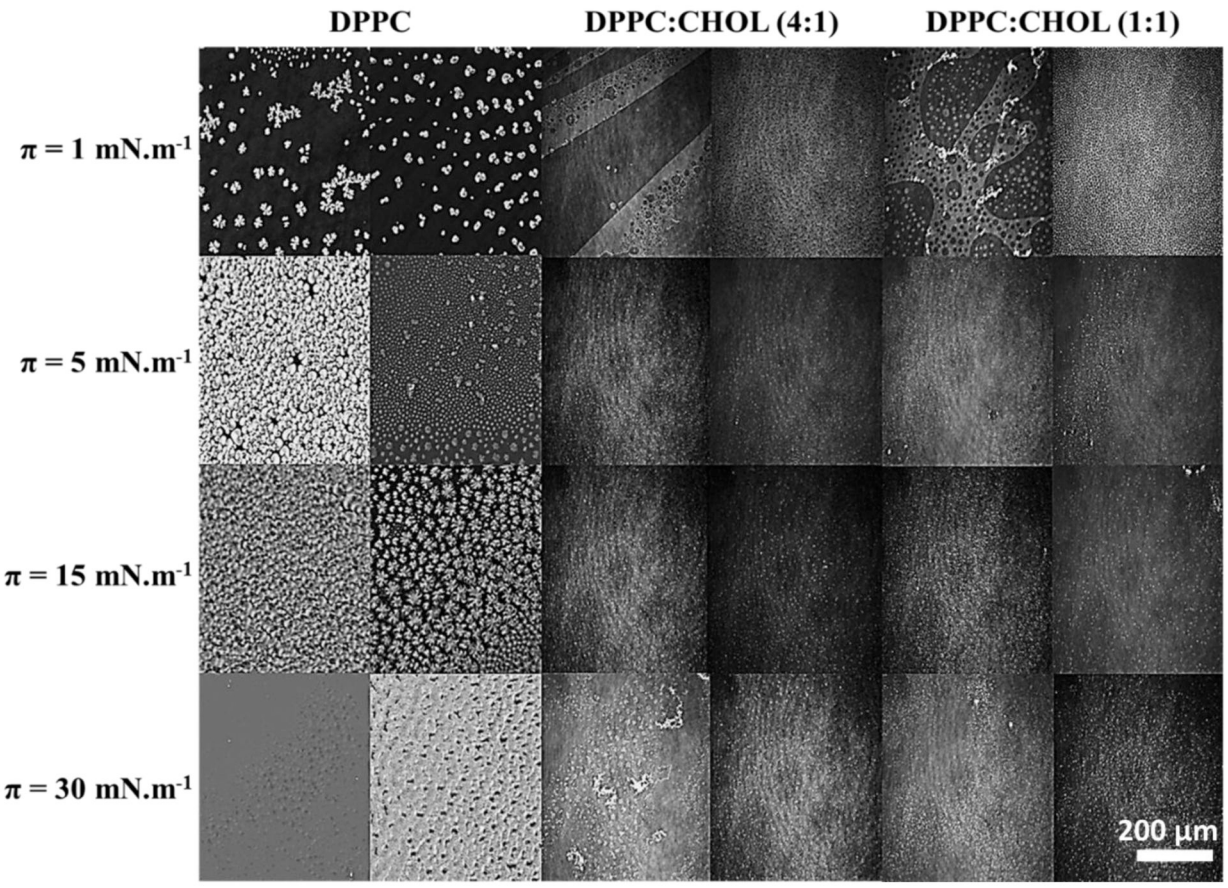

Fig. 6.

BAM micrographs of pure DPPC and DPPC:CHOL (molar ratio) mixed monolayers in absence (left column) and presence (right column) of TNAP for different π values.

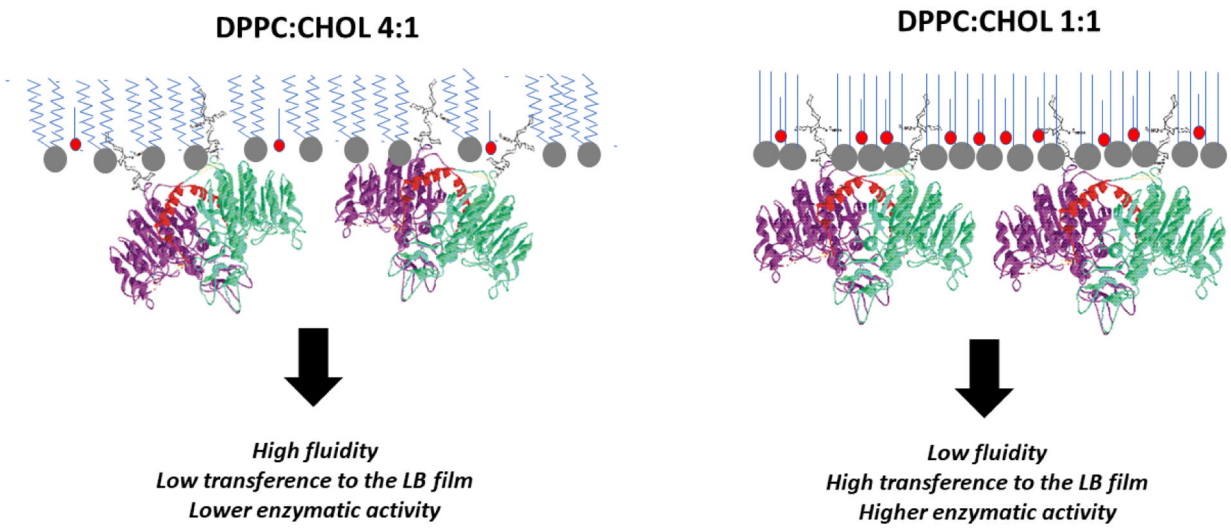

Figure 7:

Schematic representation of TNAP incorporation and orientation into DPPC:CHOL monolayers. The higher “fluidity” (compressibility) of DPPC:CHOL (4:1) compared to DPPC:CHOL (1:1) monolayer favors TNAP penetration but it hampers TNAP transfer to solid supports and decreases the catalytic activity of incorporated enzymes.

Table 1:

Characteristics of the Langmuir troughs. The compression rate was kept constant at 0.44 $mm.s^{-1}$ for all the experiments. All the TNAP-containing monolayers were obtained on 5 $mmol.L^{-1}$ Tris-HCl buffer with 150 $mmol.L^{-1}$ NaCl and 15 $mmol.L^{-1}$ $MgCl_2$ (pH 8.5) subphase, at a final enzyme concentration of 0.04 $\mu g.mL^{-1}$.

Manufacturer	Experiment	Area (cm^2)	Volume (mL)
Insight	*π-A isotherms*	216	120
PMI550	*PM-IRRAS and BAM*	225	120
Insight	*Fluorescence microscopy*	14.5	60

Table 2.

Cs^{-1} at π = 30 $mN.m^{-1}$ of the single-components and mixed monolayers (molar ratio)

Monolayer	Cs^{-1} ($mN.m^{-1}$)
DPPC	223 ± 23
DPPC:CHOL 4:1	175 ± 9
DPPC: CHOL 1:1	333 ± 26
CHOL	304 ± 20

Table 3.

The π_{exc} and Cs^{-1} calculated at $\pi=\pi_{exc}$ for the pure DPPC and mixed DPPC:CHOL monolayers

Monolayer	π_{exc} (mN.m^{-1})	Cs^{-1} (mN.m^{-1})
DPPC	12 ± 1	47± 4
DPPC:CHOL (4:1)	16 ± 2	47± 4
DPPC:CHOL (1:1)	12 ± 1	117± 8

Table 4.

Assignment of PM-IRRAS bands

Monolayer lipid composition (molar ratio)	TNAP Presence	CH_2 asym. (cm^{-1})	CH_2 sym. (cm^{-1})	C=O ester (cm^{-1})	Amide I (cm^{-1})	Amide II (cm^{-1})
DPPC	−	2920	2849	1728	-	-
DPPC	+	2915	2849	1731	1645	1562
DPPC:CHOL 4:1	−	2919	2851	1731	-	-
DPPC:CHOL 4:1	+	2913	2855	1732	1649	1534
DPPC:CHOL 1:1	−	2916	2852	1738	-	-
DPPC:CHOL 1:1	+	2916	2852	1743	*	1557

* Not observed

Table 5.

Amount of lipids deposited per layer determined using QCM and estimation of TNAP content from de difference in the area at π= 30 mN.m^{-1} of the DPPC:CHOL and DPPC:CHOL/TNAP isotherms

Monolayer lipid composition	TNAP	Total mass (ng)	TNAP mass (ng)	TNAP specific activity (U/mg)
DPPC	−	177 ± 24		-
DPPC	+	135 ± 20	21	221
DPPC:CHOL (4:1)	−	232 ± 23		-
DPPC:CHOL (4:1)	+	98 ± 21	8	129
DPPC:CHOL (1:1)	−	119 ± 24		-
DPPC:CHOL (1:1)	+	188 ± 22	59	203